Ab Initio Studies on the Photophysics of Guanine Tautomers: Out-of-Plane Deformation and NH Dissociation Pathways to Conical Intersections

Shohei Yamazaki* and Wolfgang Domcke

Department of Chemistry, Technical University of Munich, D-85747 Garching, Germany

Received: March 31, 2008; Revised Manuscript Received: May 9, 2008

The radiationless decay mechanisms of the S_1 excited states of the 7H-keto-amino, 7H-enol-amino, and 7H-keto-imino tautomers of guanine have been investigated with the CASPT2//CASSCF method. Out-of-plane deformation of the six-membered ring or the imino group as well as dissociation of NH bonds have been considered as photochemical pathways leading to conical intersections with the electronic ground state. It has been found that all three tautomers can reach S_0-S_1 conical intersections by out-of-plane deformation. However, only in the 7H-keto-amino tautomer the reaction path leading to the conical intersection is barrierless. This tautomer also has the lowest energy barrier for hydrogen detachment via the $^1\pi\sigma^*$ state, whose potential energy surface intersects that of the $^1\pi\pi^*$ state as well as that of the ground state. The other tautomers of guanine exhibit substantial energy barriers on their S_1 potential energy surfaces with respect to both reaction mechanisms. These findings suggest that the 7H-keto-amino tautomer exhibits the shortest excited-state lifetime of the three tautomers due to particularly fast nonradiative deactivation processes through S_0-S_1 conical intersections. The computational results explain the remarkable observation that the energetically most stable 7H-keto-amino tautomer is missing in the resonant two-photon ionization spectrum of guanine in a supersonic jet. The results also explain that the energetically less stable 7H-enol-amino and 7H-keto-imino tautomers have longer excited-state lifetimes and are thus detectable by resonant two-photon ionization.

1. Introduction

The understanding of the primary mechanisms of the photophysics and photochemistry of the nucleic acid bases adenine, cytosine, guanine, thymine, and uracil is an essential prerequisite for the rationalization of the photostability of DNA and RNA and the mechanisms of radiation damage. Although the nucleobases strongly absorb UV light, the quantum yields of photochemical reaction products are very low.[1] This suggests that photochemical reactions are efficiently quenched by ultrafast nonradiative decay processes back to the electronic ground state, which provide DNA with a high degree of photostability.[2] Indeed, the DNA and RNA bases exhibit very short excited-state lifetimes in the gas phase and in solution.[2] In the case of guanine, an exponential decay of the excited state with a lifetime of less than 1 ps has been observed in the gas phase.[3,4]

The electronic spectra of isolated guanine have been extensively studied using resonant two-photon ionization (R2PI) spectroscopy.[5–11] Guanine is special among the nucleobases insofar as numerous tautomers exist (36 in total, including the rotamers of the enol and imino groups). According to calculations, the four most stable tautomers in the gas phase (7H-keto-amino, 9H-keto-amino, syn-9H-enol-amino, and anti-9H-enol-amino) have energies within 1 kcal/mol.[12–15] Therefore, guanine exhibits a complicated R2PI spectrum consisting of four overlapping components, each of which originates from a different tautomer. By comparison of the IR−UV double resonance spectrum with ab initio calculated vibrational frequencies, the four bands named as A, B, C, and D were attributed to the 7H-enol-amino (syn), 7H-keto-amino, 9H-keto-amino, and 9H-enol-amino (anti) tautomers,[9,11] respectively. Recently, Choi and Miller[16] reported the IR spectra of guanine in helium nanodroplets. The spectra were assigned to a mixture of the four most stable tautomers of guanine, i.e., 9H-keto-amino, 7H-keto-amino, and two 9H-enol-amino (syn and anti) forms.[16] Surprisingly, the IR spectra of the keto-amino tautomers disagreed with the IR−UV spectra of the B and C forms. Mons et al.[17] therefore reassigned the B and C bands of the R2PI spectrum to two less stable 7H-keto-imino (E and Z) tautomers instead of the keto-amino forms. The new assignment to the 7H-keto-imino tautomers has been supported by subsequent experiments.[18,19] The missing of the most stable keto-amino tautomers in the R2PI spectra indicates that particularly fast radiationless decay processes render the lifetime of the excited states of these tautomers too short to allow the detection of an R2PI signal.

Many computational studies of the excited states of the DNA and RNA bases and their derivatives have been performed in order to elucidate the underlying mechanisms of the ultrafast decay.[20–59] Nowadays, it is widely accepted that conical intersections (CIs) are efficient funnels for the radiationless decay of photoexcited molecules to the ground state.[60–64] For the DNA bases, it has been proposed that CIs between the ground state and the $^1\pi\pi^*$ or $^1n\pi^*$ excited states are reached by out-of-plane deformations of the six-membered ring and that the nonradiative decay through these intersections is responsible for the ultrashort excited state lifetime.[20,23,26,28–31,33,37–41,44–47,53,55,59] In the case of adenine, it has also been shown that the potential energy (PE) function of an excited state of $^1\pi\sigma^*$ character intersects the $^1\pi\pi^*$ state as well as the ground state via the dissociation of an NH bond and thus provides an additional pathway for the ultrafast decay.[21,22,28,30,34]

Most of the theoretical studies on the photochemistry of guanine have been focused on the biologically relevant 9H-keto-amino tautomer. Out-of-plane-type CIs of this tautomer

* To whom correspondence should be addressed. E-mail: yamazaki@ch.tum.de.

10.1021/jp802759v CCC: $40.75
Published on Web 07/10/2008

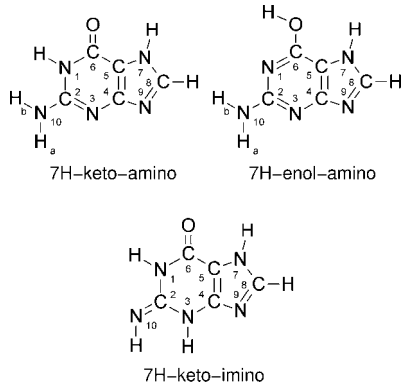

Figure 1. Structures of 7H-guanine tautomers.

have been located by several authors.[44,53,59] The PE surface leading from the Franck−Condon (FC) region to the CI between the ground state and the lowest $^1\pi\pi^*$ state has been calculated using the complete-active-space self-consistent-field (CASSCF) method and second-order perturbation theory based on the CASSCF reference (CASPT2).[44,59] The calculated energy profile indicates a barrierless reaction path to the S_0-S_1 CI, which is consistent with an extremely short excited-state lifetime of 9H-keto-amino guanine and the missing of this tautomer in the R2PI spectrum. The PE profile of the $^1\pi\sigma^*$ state along the NH bond of the 9H-keto-amino tautomer was also reported.[44]

Theoretical studies of the excited states of the other tautomers of guanine are still limited. Several excited-state minima and CIs have been located for some of them,[45,53,59] and PE profiles between the FC region and the CIs have been obtained by Serrano-Andrés et al.[59] for several 9H and 7H tautomers. The $^1\pi\sigma^*$ -driven dissociation mechanism of 7H-guanine tautomers has been studied by excited-state nonadiabatic Car−Parrinello simulations in aqueous solution.[35]

In the present work, we have examined the out-of-plane deformation mechanism as well as the NH dissociation mechanism for three selected tautomers of guanine using the CASPT2//CASSCF method. As mentioned above, while the 7H-enol-amino and 7H-keto-imino tautomers have been detected in the R2PI experiment, the more stable 7H-keto-amino form has not been observed. It is therefore of particular interest to compare the photophysics of keto-amino, enol-amino, and keto-imino tautomers of guanine. We have selected the 7H-keto-amino, 7H-enol-amino (syn), and 7H-keto-imino (E) conformers for this purpose. The structures of these tautomers are shown in Figure 1.

2. Computational Details

The calculations of the present work were carried out with the MOLPRO[65] program package. The CASSCF method was used for the optimization of excited-state minima and CIs between the ground state and excited states. The ground-state geometry was optimized with the second-order Møller−Plesset perturbation (MP2) method. For the geometry optimizations, we employed the (9s5p1d/4s1p)/[3s2p1d/2s1p] basis set,[66] which is of double-ζ plus polarization quality. For the calculation of the $^1\pi\sigma^*$ state, this basis set was further augmented with diffuse s and p basis functions[66] on all N and O atoms. The exponents of the s and p functions are 0.028 and 0.025, respectively, for N and 0.032 and 0.028 for O. For the calculation of excited-state reaction paths and energy profiles, we chose one internal degree of freedom (a dihedral angle or an NH bond length) as the driving coordinate and optimized the other internal coordinates. In the CASSCF calculations, state averaging was carried out over two states (the ground state and the target excited state) with equal weights. For the NH dissociation pathways, the geometry optimizations were performed with C_s symmetry restriction. The other geometries were optimized without any symmetry constraint.

In the CASSCF optimizations, we used several active spaces for different electronic states and reaction paths. For the out-of-plane deformation pathways of the 7H-keto-amino and 7H-keto-imino tautomers, the active space was constructed by distributing 16 electrons in 12 orbitals, consisting of 11 π orbitals and one lone pair orbital at the N atom (N_3 for 7H-keto-amino and N_{10} for 7H-keto-imino; see Figure 1 for the atom labeling). In the case of the 7H-enol-amino tautomer, we employed the active space of 12 electrons distributed in 10 orbitals, because the optimizations with 12 active orbitals could not be properly converged due to the mixing of the orbitals. For the same reason, several sets of active orbitals were used for the optimizations of different structures. We adopted 10 π orbitals for the $^1\pi\pi^*$ state minimum. For the CI referred to as CI_{32} (see section 3.2 for the labeling of CIs), the lowest π orbital was replaced by the lone pair orbital on the N_3 atom. An additional π orbital was replaced by the N_1 lone pair orbital for the CI labeled as CI_{16}. The $^1\pi\pi^*$ PE curves along the NH dissociation pathways of the three tautomers were calculated with an active space of 14 electrons and 11 π orbitals. For the $^1\pi\sigma^*$ state, one σ^* Rydberg orbital was added to the active space.

Single-point internally contracted CASPT2 calculations[67] were performed at the optimized geometries to account for dynamical electron correlation effects. A level shift with the parameter 0.3 was employed.[68] For the out-of-plane deformation pathways of the three tautomers, the CASPT2 energies were calculated with the (10s6p1d/5s1p)/[5s3p1d/3s1p] basis set,[69] which has triple-ζ plus polarization quality, and an active space of 16 electrons distributed in 12 orbitals. The active spaces for the 7H-keto-amino and 7H-keto-imino tautomers are the same as those in the CASSCF optimizations. The active orbitals for the 7H-enol-amino tautomer consist of 10 π orbitals and 2 lone pair orbitals on the N_1 and N_3 atoms. The underlying CASSCF wave functions were obtained with averaging of the lowest four singlet states with equal weights. For the NH dissociation pathways, we employed the triple-ζ basis set augmented with the same diffuse functions[66] as used for the CASSCF optimizations with the double-ζ basis set. The active space consists of 14 electrons and 12 orbitals (11 π orbitals and one σ^* orbital). In the underlying CASSCF calculations, the ground state and the lowest $^1\pi\pi^*$ and $^1\pi\sigma^*$ states were averaged with the same weight.

We also calculated the vertical excitation energies of the three tautomers at the ground-state equilibrium geometries with the CASPT2 method. The $^1\pi\pi^*$ and $^1n\pi^*$ energies were obtained with active spaces of 16 electrons and 12 orbitals, where the in-plane lone pair orbitals on the N atoms of the 7H-keto-amino and 7H-keto-imino tautomers were replaced by those on the O atom. The $^1\pi\sigma^*$ excitation energies were calculated with the same active space and state averaging as for the NH dissociation pathways.

The CASPT2 energies of two crossing states at the CASSCF-optimized CI geometry may be different due to the difference of the dynamical electron correlation energies of the two states. To locate the crossing point at the CASPT2 level, the CI geometry was corrected by a displacement in the direction of

TABLE 1: Vertical Excitation Energies (ΔE_{vert}), Oscillator Strengths (f), and Dipole Moments (μ) of the Ground State and the Low-Lying Singlet Excited States of Guanine Tautomers, Obtained at the CASPT2//CASSCF Level

state	ΔE_{vert}/eV	f	μ/D
7H-keto-amino			
S_0			1.9
$^1\pi\pi^*$ (^1L_a)	4.37	0.142	3.4
$^1\pi\pi^*$ (^1L_b)	5.11	0.009	2.1
$^1n_O\pi^*$	5.24	0.001	5.2
$^1\pi\sigma^*$	5.09	0.003	12.0
7H-enol-amino			
S_0			4.1
$^1\pi\pi^*$ (^1L_a)	4.21	0.067	2.7
$^1\pi\pi^*$ (^1L_b)	5.12	0.064	5.5
$^1n_N\pi^*$	4.94	0.011	2.8
$^1\pi\sigma^*$	5.24	0.000	12.1
7H-keto-imino			
S_0			3.8
$^1\pi\pi^*$ (^1L_a)	4.33	0.087	4.7
$^1\pi\pi^*$ (^1L_b)	5.13	0.022	4.1
$^1n_O\pi^*$	5.10	0.000	3.1
$^1\pi\sigma^*$	4.93	0.001	11.5

the gradient difference vector. The displacement vector Δx for a CI between the states I and J was estimated by[51]

$$\Delta x = -\frac{\Delta E^{IJ}}{|\mathbf{g}^{IJ}|^2}\mathbf{g}^{IJ} \quad (1)$$

where ΔE^{IJ} is the energy difference at the CASPT2 level and $\mathbf{g}^{IJ}$ is the gradient difference vector at the CASSCF level.

3. Results and Discussion

3.1. Vertical and Adiabatic Excitation Energies. The ground-state equilibrium structures of the 7H-keto-amino and 7H-enol-amino tautomers optimized at the MP2 level are almost planar except of a slight pyramidalization of the amino group. In the case of the 7H-keto-imino tautomer, the optimized structure is completely planar. The Cartesian coordinates of these structures as well as those of the other structures optimized in this work are given in the Supporting Information.

The CASPT2 vertical excitation energies of the low-lying singlet excited states at the MP2-optimized geometries are given in Table 1. The oscillator strengths and the CASSCF dipole moments of the ground and excited states are also included. For all three tautomers, the $^1\pi\pi^*$ (^1L_a) state is the lowest excited-state and has the largest oscillator strength among the states under consideration. Hence, this state dominates the near-UV photoabsorption spectrum of guanine. The $^1\pi\pi^*$ (^1L_b), $^1n\pi^*$, and $^1\pi\sigma^*$ states lie higher in energy by more than 0.5 eV. The lowest $^1n\pi^*$ state of the 7H-keto-amino and 7H-keto-imino tautomers corresponds to the excitation from the lone pair orbital on the O atom. For the 7H-enol-amino tautomer, the $^1n\pi^*$ state results from the excitation from the lone pair orbital on the N atom in the six-membered ring. Details of the wave functions of the $^1\pi\sigma^*$ states are discussed in section 3.3.

We also optimized the equilibrium geometry of the lowest $^1\pi\pi^*$ (^1L_a) state at the CASSCF level. For the 7H-enol-amino and 7H-keto-imino tautomers, potential energy minima with planar structures were located. The adiabatic excitation energies of these two tautomers calculated at the CASPT2 level are given in Table 2. The calculated adiabatic excitation energies of the 7H-enol-amino and 7H-keto-imino tautomers are 3.92 and 4.12 eV, respectively. They are in a good agreement with the origin lines in the R2PI spectra of tautomers A (4.07 eV) and C (4.20 eV)[17] and the previous theoretical results.[45,53,59] In our CASSCF geometry optimization of the lowest $^1\pi\pi^*$ (^1L_a) state, no energy minimum was found for the 7H-keto-amino tautomer. This is different from the previous studies, in which a potential energy minimum of this tautomer was located at either a nearly planar geometry or a highly out-of-plane deformed geometry.[45,53,59] This discrepancy with earlier work most likely is due to difference of computational levels (basis set, active space, and electron-correlation treatment).

TABLE 2: Adiabatic Excitation Energies of the $^1\pi\pi^*$(^1L_a) State (ΔE_{adia}) and S_0-S_1 CI Energies (E_{CI}) of Guanine Tautomers, Obtained at the CASPT2 Level

	ΔE_{adia}/eV		
tautomer	calc.	exp.[a]	E_{CI}/eV[b]
7H-keto-amino			4.02 (CI_{32})
7H-enol-amino	3.92	4.07	4.04 (CI_{32}), 4.11 (CI_{16})
7H-keto-imino	4.12	4.20	3.73 (CI_{210} −a), 3.73 (CI_{210} −b)

[a] Reference 17. [b] Measured from the energy of the ground-state minimum.

The results for the vertical excitation energies suggest that the three 7H-guanine tautomers are excited to the $^1\pi\pi^*$ (^1L_a) state by photoabsorption. The nonadiabatic transitions from this state to the ground state or other excited states are essentially involved in the excited-state dynamics. In following sections, we discuss two mechanisms of radiationless decay from this state, namely the out-of-plane-deformation and bond-dissociation pathways. Hereafter, the $^1\pi\pi^*$ (^1L_a) state is denoted as the $^1\pi\pi^*$ state for brevity.

3.2. Out-of-Plane Deformation Pathways. Needless to say, the existence of CIs between the electronic ground-state surface and the lowest excited-state PE surface, i.e., S_0-S_1 CIs, is essential for the ultrafast radiationless decay of photoexcited molecules. Previous theoretical studies for the DNA and RNA bases[20,23,26,28–31,33,37–41,44–47,53,55,59] and the guanine−cytosine base pair[70] have revealed the existence of such CIs induced by out-of-plane deformations of the six-membered ring, characterized by the twisting of C−C or C−N double bonds in the ring.

The 7H-keto-amino and 7H-enol-amino tautomers of guanine have N_3C_2 and C_4C_5 double bonds of the six-membered ring in the ground state, see Figure 1. Since the twisting of the latter bond is hindered by the five-membered ring, the N_3C_2 bond is the primary candidate for twisting. Starting the optimizations with N_3C_2-twisted structures, we located S_0-S_1 CIs in the two tautomers at the CASSCF level. To obtain the CI structures at the CASPT2 level, the CASSCF-optimized geometries were further corrected as explained in section 2. The CASPT2 energy gaps of about 0.5 eV at the CASSCF geometries were reduced to less than 0.3 eV by the correction. Figure 2, panels a and b, shows the corrected geometries of the CIs, referred to as CI_{32}, of the two tautomers, respectively. The 7H-enol-amino tautomer has an additional N_1C_6 double bond, see Figure 1. A CI optimization of this tautomer was additionally started with an N_1C_6-twisted structure and the geometry as shown in Figure 2c was obtained. This CI is referred to as CI_{16}.

As is expected, the N_3C_2 bond is strongly twisted at the CI_{32}. The values of the dihedral angle $\delta(C_4N_3C_2N_1)$ at the CI_{32} geometries of the 7H-keto-amino and 7H-enol-amino tautomers are 71.1° and 65.5°, respectively. The twisting of the N_3C_2 bond results in a large out-of-plane distortion of the amino group. The dihedral angle $\delta(C_4N_3C_2N_{10})$ is −146.6° for the 7H-keto-amino tautomer and −73.6° for the 7H-enol-amino tautomer. The CI_{16} of the 7H-enol-amino tautomer has a strongly twisted

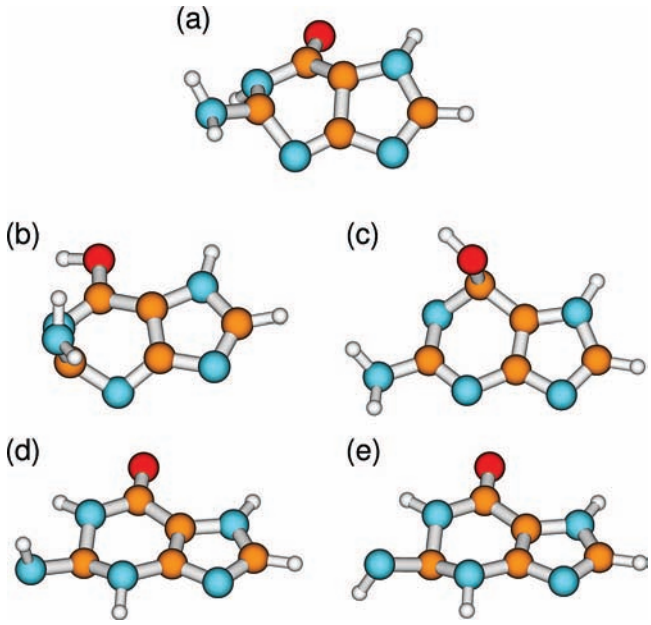

Figure 2. Optimized CI geometries (after correction by eq 1) of three guanine tautomers: (a) CI_{32} of 7H-keto-amino, (b) CI_{32} of 7H-enol-amino, (c) CI_{16} of 7H-enol-amino, (d) CI_{210}−a of 7H-keto-imino, and (e) CI_{210}−b of 7H-keto-imino.

N_1C_6 bond, as shown by the dihedral angle $\delta(C_2N_1C_6C_5) = 54.6°$. As a result, the hydroxyl group at the CI_{16} is strongly twisted out of plane, the dihedral angle being $\delta(C_2N_1C_6O) = -72.1°$.

Although the 7H-keto-imino tautomer of guanine has no double bond in the six-membered ring other than the locked C_4C_5 bond, it has the C_2N_{10} double bond of the imino group, see Figure 1. Starting the optimization with C_2N_{10}-twisted structures, we found two S_0-S_1 CI structures of this tautomer. The obtained geometries are shown in Figure 2, panels d and e, where these CIs are labeled as CI_{210}−a and CI_{210}−b, respectively. The two CI_{210} structures correspond to opposite directions of the C_2N_{10} twisting. For both CIs, the C_2 atom of the six-membered ring undergoes a slight out-of-plane distortion with respect to the other five atoms at these CI geometries. The $N_{10}H$ bond of the CI_{210}−a is directed opposite to the C_2 distortion, whereas that of the CI_{210}−b is in the same direction. The dihedral angle $\delta(N_3C_2N_{10}H)$ has the values +65.9° and −120.8° at the CI_{210}−a and CI_{210}−b, respectively.

The CASPT2 energies of these CIs are included in Table 2. All CI energies are in a narrow range around 4.0 eV from the ground-state minimum. These energies are close to the adiabatic excitation energies of the $^1\pi\pi^*$ state and lower than the vertical excitation energies. Therefore, for all three tautomers, the possibility of ultrafast internal conversion from the $^1\pi\pi^*$ state through the CIs is not excluded by their energies.

To judge the accessibility of the CIs, it is essential to know whether or not a significant energy barrier exists between the FC region and each of the CIs. To explore this issue, we calculated the excited-state PE functions corresponding to the coordinate-driven minimum-energy reaction paths from the FC region to the five CIs. For this purpose, the dihedral angle characterizing the respective CI was selected as the driving coordinate: $\delta(C_4N_3C_2N_1)$ for the CI_{32}, $\delta(C_2N_1C_6C_5)$ for the CI_{16}, and $\delta(N_3C_2N_{10}H)$ for the CI_{210}. Starting with the ground-state equilibrium geometry, the dihedral angle is fixed at different values, while the $^1\pi\pi^*$ energy is optimized with respect to the other internal degrees of freedom.

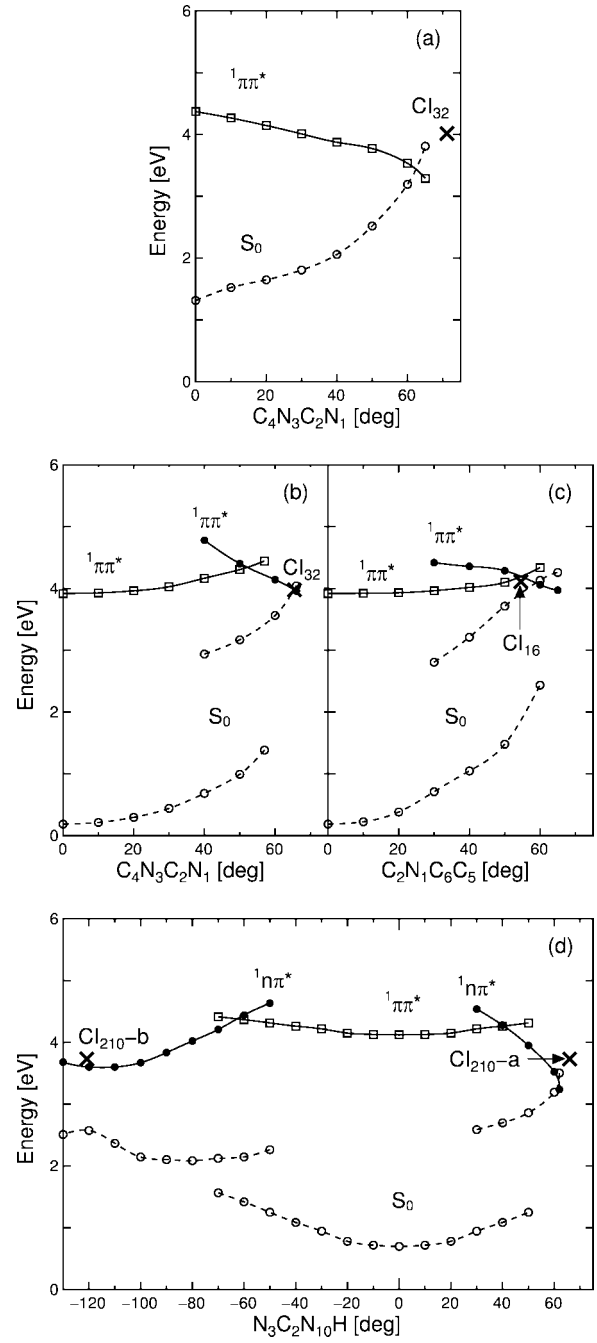

Figure 3. CASPT2 PE functions of the ground state (S_0; open circles), the $^1\pi\pi^*$ state (open squares), and the biradical $^1\pi\pi^*$ or $^1n\pi^*$ states (filled circles) of guanine tautomers along out-of-deformation pathways leading to CIs: (a) CI_{32} of 7H-keto-amino, (b) CI_{32} of 7H-enol-amino, (c) CI_{16} of 7H-enol-amino, (d) CI_{210}−a and CI_{210}−b of 7H-keto-imino. Full lines indicate the energies of the excited states at their CASSCF-optimized geometries. Dashed lines show the energies of the ground-state at the excited-state geometries. Crosses indicate the optimized S_0-S_1 CI points (after correction by eq 1).

The resulting CASPT2 energy profiles are shown in Figure 3. The full curve with open squares represents the energy profile of the $^1\pi\pi^*$ excited state along the reaction path. The dashed curve with circles gives the ground-state energy, calculated at the $^1\pi\pi^*$-optimized geometries. For the 7H-keto-amino tautomer, a barrierless pathway leading toward the CI_{32} was obtained, see Figure 3a. As mentioned above, no energy minimum of the $^1\pi\pi^*$ state could not be found in the present calculations. These findings suggest that the radiationless decay takes place very efficiently through the CI_{32} for the photoexcited

7H-keto-amino tautomer, which explains the absence of this tautomer in the R2PI spectrum. An analogous barrierless PE profile has also been obtained for the 9H-keto-amino tautomer,[44,59] which also is missing in the R2PI spectrum.[17–19] Note that, apart from the optimized CI_{32} point at $\delta(C_4N_3C_2N_1) = 71.1°$ (cross in Figure 3a), there is an S_0-S_1 curve crossing along the PE function at about $\delta(C_4N_3C_2N_1) = 62°$. Both are points on a multidimensional seam of intersection of the S_1 and S_0 states. As seen in Figure 3a, the CASSCF-optimized CI_{32} lies higher in energy than this CASPT2 curve crossing. This finding is a computational artifact resulting from the fact that the CI is not fully optimized at the CASPT2 level. It should be noticed that the geometry correction by eq 1 only reduces the CASPT2 energy difference of the two crossing states, but does not yield the minimum-energy point of the crossing seam.

The coordinate-driven reaction paths of the 7H-enol-amino and 7H-keto-imino tautomers whose optimizations start at the FC region are shown as the curves with open squares in Figure 3b–d. The 0° points of these curves correspond to the $^1\pi\pi^*$ minima of the two tautomers and thus their energies correspond to the adiabatic excitation energies given in Table 2. The excited-state energies increase monotonically along the reaction coordinates and the paths do not lead to an S_0-S_1CI. Therefore, we also performed reaction-path optimizations starting at the CI geometries and leading back toward the FC region for these two tautomers. The resulting energy profiles are shown as the curves with filled circles in the figures. They exhibit crossings with the $^1\pi\pi^*$ energy profiles obtained by starting from the FC region. It follows that the S_1 PE surfaces of the 7H-enol-amino and 7H-keto-imino tautomers have substantial energy barriers separating the FC region from the CIs. Note that these crossings are apparent crossings, since the points of the two curves at each value of the reaction coordinates correspond to different geometries. The barriers of the PE surfaces are predicted to be higher in energy than these apparent curve crossings. The largest difference between the geometries along the two PE curves (open squares and filled circles) is observed for the out-of-plane distortion of the amino group, the hydroxy group, and the C_2 atom on the six-membered ring for CI_{32}, CI_{16}, and CI_{210}, respectively. These distortions are very small for the $^1\pi\pi^*$ reaction paths starting at the FC region, while they are much larger for the reaction paths starting at the CIs. As in the case of the CI_{32} of the 7H-keto-amino tautomer, true S_0-S_1 curve crossings were confirmed near the CI_{32} and CI_{16} of the 7H-enol-amino tautomer and the CI_{210}–a of the 7H-keto-imino tautomer. Such a crossing could not be found along the reaction path toward the CI_{210}–b. The optimization rather reached an S_1 energy minimum at about $\delta(N_3C_2N_{10}H) = -120°$.

The electronic states at the CIs and their vicinity are of biradical character, as has been pointed out previously for the 9H-keto-amino tautomer.[44,59] The dominant configuration of the lowest excited state at the CI_{32} geometry of the 7H-keto-amino and 7H-enol-amino tautomers, labeled as $^1\pi\pi^*$, corresponds to the excitation from the p orbital localized mainly on N_3 and C_5 to that centered on C_2. In the case of the CI_{16} of the 7H-enol-amino tautomer, the excitation from the p orbital on N_1 to that on C_6 dominates the lowest excited state, which is also of $^1\pi\pi^*$ character. The first excited state at the CI_{210} geometries of the 7H-keto-imino tautomer is of $^1n\pi^*$ character. It primarily results from the excitation from the p orbital on the N_{10} atom to the p orbital on the C_{10} atom. Molecular orbitals involved in these excitations are shown in the Supporting Information.

3.3. NH Dissociation Pathways. The radiationless decay mechanism via the dissociation of an NH or OH bond in the $^1\pi\sigma^*$ states has been proposed for molecules such as adenine,[21,22,28,30,34] indole,[71] pyrrole,[72] and phenol.[73] The PE profile with respect to this mechanism was examined for the 9H-keto-amino tautomer[44] but not for other tautomers of guanine. In this section, we discuss the $^1\pi\sigma^*$ mechanism for the three respective 7H tautomers.

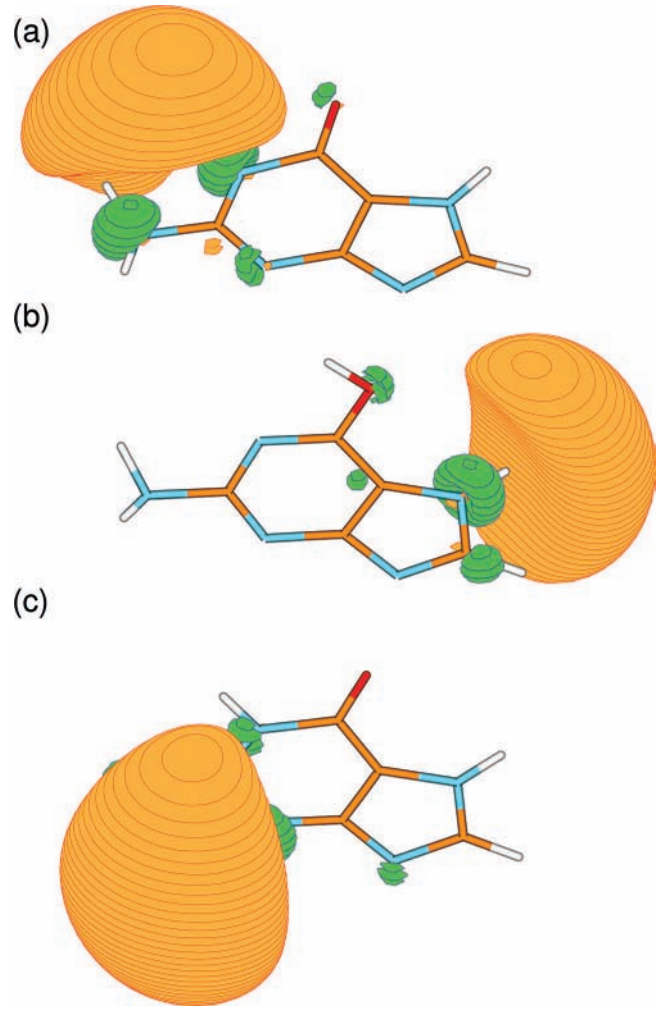

Figure 4. σ^* orbitals at the ground-state equilibrium geometries of three guanine tautomes: (a) 7H-keto-amino, (b) 7H-enol-amino, and (c) 7H-keto-imino.

The results for the vertical excitation energy of the lowest $^1\pi\sigma^*$ state at the CASPT2 level are included in Table 1. As mentioned in section 3.1, the lowest $^1\pi\sigma^*$ state lies higher in energy than the lowest $^1\pi\pi^*$ state and has a very low oscillator strength. The $^1\pi\sigma^*$ states of the three tautomers have 3s Rydberg character in the FC region. Figure 4 shows the diffuse σ^* orbitals of the three tautomers obtained by CASSCF calculations at the ground-state equilibrium geometries. For the 7H-keto-amino tautomer, the σ^* orbital is covering the N_1H bond of the six-membered ring as well as the $N_{10}H_b$ of the amino group (Figure 4a). A σ^* orbital of similar shape has been obtained for the 9H-keto-amino tautomer.[53] The σ^* orbital of the 7H-enol-amino tautomer is located on the N_7H bond of the five-membered ring, see Figure 4b. The $^1\pi\sigma^*$ state associated with the OH bond of 7H-enol-amino guanine lies higher in energy than the $^1\pi\sigma^*$ state associated with the N_7H bond. For the 7H-keto-imino tautomer, the σ^* orbital covers the N_3H bond of the six-membered ring as well as the $N_{10}H$ bond of the imino group, see Figure 4c. As a consequence of the localization of charge outside the molecular frame in the σ^* orbitals, the $^1\pi\sigma^*$ states of the three tautomers

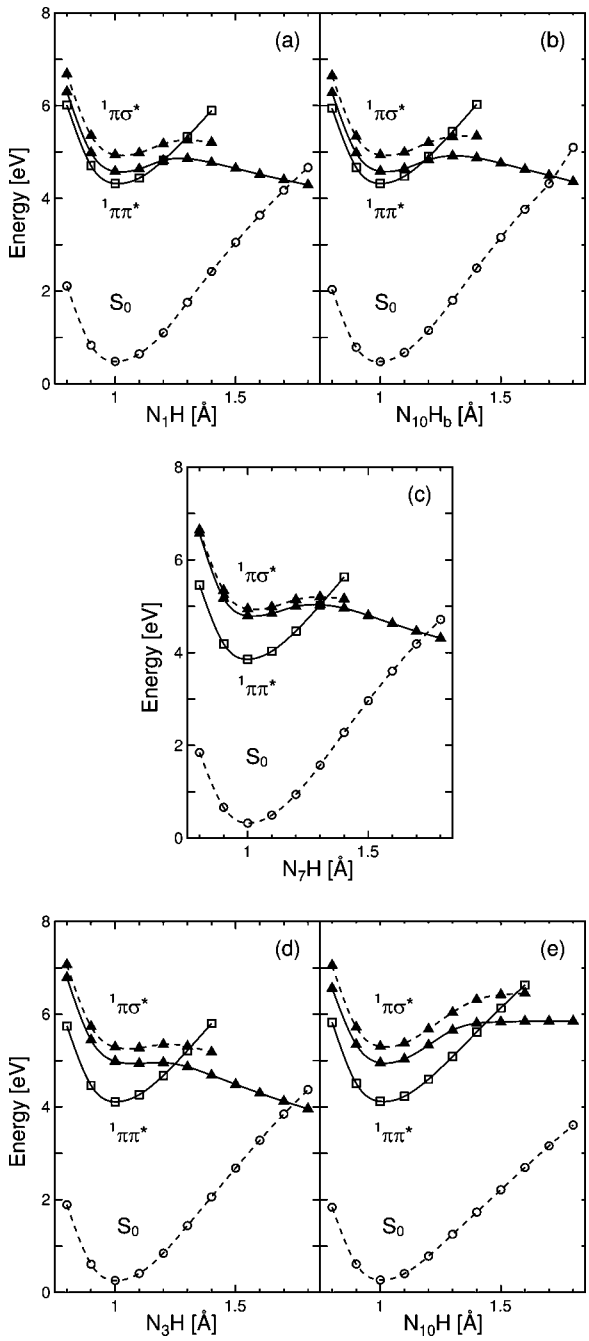

Figure 5. CASPT2 PE functions of the ground state (S_0; open circles), the $^1\pi\pi^*$ state (open squares), and the $^1\pi\sigma^*$ state (filled triangles) of guanine tautomers along dissociation pathways of NH bonds: (a) N_1H of 7H-keto-amino, (b) $N_{10}H_b$ of 7H-keto-amino, (c) N_7H of 7H-enol-amino, (d) N_3H of 7H-keto-imino, and (e) $N_{10}H$ of 7H-keto-imino. Full lines indicate the energies of the excited states calculated at their CASSCF-optimized geometries, while dashed lines show the energies of the ground state at the $^1\pi\sigma^*$-optimized geometries and the energies of the $^1\pi\sigma^*$ state at the $^1\pi\pi^*$-optimized geometries.

have much larger dipole moments than the ground state and other excited states. As seen in Table 1, the dipole moments of the $^1\pi\sigma^*$ states of the 7H-keto-amino, 7H-enol-amino, and 7H-keto-imino tautomers are 12.0, 12.1, and 11.5 D, respectively, at the ground-state equilibrium geometries.

Figure 5 shows the CASPT2 PE functions of the $^1\pi\pi^*$ and $^1\pi\sigma^*$ states as functions of the NH bond lengths, that is, the N_1H and $N_{10}H_b$ bonds of the 7H-keto-amino tautomer, the N_7H bond of the 7H-enol-amino tautomer, and the N_3H and $N_{10}H$ bonds of the 7H-keto-imino tautomer. The NH-stretching reaction paths were optimized in the $^1\pi\sigma^*$ excited states (full curves with triangles). The ground-state energies calculated at the $^1\pi\sigma^*$-optimized geometries (dashed curves with circles) and the $^1\pi\pi^*$ and $^1\pi\sigma^*$ energies calculated at the $^1\pi\pi^*$-optimized geometries (full curves with squares and dashed curves with triangles, respectively) are also shown in the figure. At small values of the NH bond lengths, all $^1\pi\sigma^*$ PE functions exhibit an energy minimum as well as a barrier. The latter reflects the Rydberg-to-valence transformation of the σ^* orbital as in adenine,[21,22,28,30,34] the 9H-keto-amino tautomer of guanine,[44] or other molecules.[71–73] The CASPT2 adiabatic excitation energies of the 7H-keto-amino, 7H-enol-amino, and 7H-keto-imino tautomers are 4.49, 4.75, and 4.88 eV, respectively. They are higher than the adiabatic excitation energies of the $^1\pi\pi^*$ states. At larger values of the NH lengths, the σ^* orbital mainly consists of the 1s valence orbital of the detaching hydrogen atom. For both the azine and amino groups, the $^1\pi\sigma^*$ energies are repulsive as a function of the NH bond length, resulting in a crossing with the ground state at a bond length of about 1.7 Å (see Figure 5a–d). For the imino group, on the other hand, the $^1\pi\sigma^*$ energy function is flat and does not lead to a crossing with the ground state (see Figure 5e). The $S_0-{}^1\pi\sigma^*$ crossings are symmetry-allowed in planar structures, because the S_0 and $^1\pi\sigma^*$ states have $^1A'$ and $^1A''$ symmetries, respectively, in the C_s point group. When out-of-plane displacements are taken into account, these crossings become CIs.

Since the $^1\pi\pi^*$ state is the initially populated state in photoabsorption and since it is lower in energy than the $^1\pi\sigma^*$ state in the FC region, a barrier has to be overcome for the dissociation of the NH bond. The energies of the $^1\pi\pi^*-{}^1\pi\sigma^*$ state crossings in Figure 5 (full lines with squares and triangles, respectively) represent lower limits for these barriers since the energy crossings are apparent crossings. One can see that the 7H-keto-amino tautomer exhibits the lowest barriers for both NH coordinates (Figure 5a–b). The PE functions of the N_1H and $N_{10}H_b$ bonds of this tautomer are similar and the threshold for NH dissociation can be estimated to lie about 0.5 eV above the $^1\pi\pi^*$ minimum. Therefore, deactivation via the $^1\pi\sigma^*$ mechanism is most likely for the 7H-keto-amino tautomer. The crossings of the optimized $^1\pi\pi^*$ curves (full line with squares) with the $^1\pi\sigma^*$ curves at the $^1\pi\pi^*$-optimized geometries (dashed line with circles) in Figure 5, on the other hand, represent upper limits for these barriers, since they are true crossings and out-of-plane deformation lowers the barriers.

The energy difference between the $^1\pi\pi^*-{}^1\pi\sigma^*$ crossing and the $^1\pi\pi^*$ minimum of the 7H-keto-amino tautomer estimated in the present work is much smaller than the value reported for the 9H-keto-amino tautomer in ref.[44] This may result from the fact that the NH dissociation energies of the present study were calculated with C_s symmetry constraint, whereas the energy functions in ref[44] were obtained with no symmetry restriction. This is particularly relevant for the energy of the $^1\pi\pi^*$ state. Note that the $^1\pi\pi^*$ minimum obtained in ref 44 is very near to the S_0-S_1 CI of out-of-deformation type. The $^1\pi\pi^*$ PE surface of the 9H-keto-amino tautomer within C_s symmetry is expected to be similar to that of the 7H-keto-amino tautomer.

It should also be noted that the energy minimum on the $^1\pi\pi^*$ state of the 7H-keto-amino tautomer in Figure 5a,b is in fact a saddle point rather than a true minimum. The energy of this state will decrease by out-of-plane deformation, as shown in Figure 3a. Therefore, the NH dissociation mechanism and the out-of-plane deformation mechanism are competing channels in the radiationless decay of the $^1\pi\pi^*$ state of the 7H-keto-amino tautomer. At excitation energies which are lower than

the minimum energy of the $^1\pi\pi^*-^1\pi\sigma^*$ crossing, decay via the out-of-plane deformation mechanism is more likely.

The 7H-enol-amino and 7H-keto-imino tautomers exhibit significant energy barriers between the $^1\pi\pi^*$ minimum and the $S_0-^1\pi\sigma^*$ crossing, as shown in Figure 5c−e. For the PE function of the N_7H bond of the 7H-enol-amino tautomer, the $^1\pi\pi^*-^1\pi\sigma^*$ apparent crossing lies about 1.2 eV higher in energy than the $^1\pi\pi^*$ minimum. The true crossing is at similar energy (about 1.3 eV above the $^1\pi\pi^*$ minimum). For the N_3H and $N_{10}H$ bonds of the 7H-keto-imino tautomer, the barrier heights can be estimated to be about 0.8 and 1.7 eV, respectively. The $^1\pi\pi^*$ minima of the two tautomers are true minima and therefore out-of-plane deformation induces no energy decrease. These results indicate that the radiationless decay of these tautomers via the $^1\pi\sigma^*$ mechanism is less likely than that of the 7H-keto-amino tautomer.

3.4. Radiationless Decay Mechanism of 7H-Guanine Tautomers. The results described above provide a qualitative explanation of the unexpected absence of the keto-amino tautomers of guanine in the R2PI spectra. At the lowest excitation energies, the radiationless decay through the out-of-plane deformation pathway presumably dominates the excited-state dynamics. Since the PE function of the $^1\pi\pi^*$ state exhibits no energy barrier separating the FC region from the CI, the lifetime of this state is expected to be extremely short. At slightly higher excitation energies, the additional pathway of the $^1\pi\sigma^*$-driven dissociation of the NH bond becomes effective. For the 7H-enol-amino (syn form) and 7H-keto-imino (E form) tautomers, the PE surfaces exhibit significant energy barriers between the FC region and the CIs for both mechanisms. Therefore, these tautomers are predicted to have comparatively long excited-state lifetimes and can thus be detected in the R2PI spectrum. The adiabatic energies of the 7H-enol-amino and 7H-keto-imino tautomers given in Table 2 are consistent with the assignment of the A and C band origins in the R2PI spectrum, respectively, to the $^1\pi\pi^*$ origins of the enol-amino and keto-imino tautomers.[17] Recent computational studies[18,45,53] also support this assignment.

We also comment on the Z form of the 7H-keto-imino tautomer, which has been proposed as the carrier of band B of the R2PI spectrum.[17] The only structural difference between the E and Z forms is the direction of the NH bond of the imino group. At the ground-state geometry, the value of the dihedral angle $\delta(N_3C_2N_{10}H)$ is 0° for the E form, whereas it is 180° for the Z form. Therefore, it is likely that the Z form exhibits excited-state PE surfaces which are similar to the E form. In particular, it is worth noting that the Z form as well as the E form can reach the CI_{210} structures by the twisting of the C_2N_{10} bond and the out-of-plane deformation of the six-membered ring.

4. Conclusions

The radiationless decay pathways of three representative guanine tautomers, i.e., 7H-keto-amino, 7H-enol-amino, and 7H-keto-imino forms, have been examined using the CASSCF and CASPT2 methods. The excited-state reaction paths leading from the FC region to the S_0-S_1 CIs have been determined, considering both the out-of-plane deformation and the NH dissociation mechanisms. The S_0-S_1 CIs of the out-of-plane deformation type have been located for all three tautomers. The 7H-keto-amino and 7H-enol-amino tautomers can reach S_0-S_1 CIs by the puckering of the six-membered ring, whereas the S_0-S_1 CI of the 7H-keto-imino tautomer is reached by the twisting of the CN bond of the imino group. Only the 7H-keto-amino tautomer exhibits a barrierless pathway leading to the S_0-S_1 CI, as was also demonstrated for the biologically relevant 9H-keto-amino tautomer.[44,59] The keto-amino tautomer also exhibits the lowest barrier for the NH dissociation in the $^1\pi\sigma^*$ state. These findings strongly support the assumption that the missing of the 7H-keto-amino tautomer in the R2PI spectrum is due to ultrafast nonradiative excited-state deactivation through these particular pathways.

It has been postulated that the DNA bases have been selected under primordial conditions of extremely intense flux of hard UV radiation with respect to exceptionally efficient deactivation mechanisms of the excited electronic states, which minimize the yield of destructive photochemical reactions.[2,74–76] The unexpected absence of an R2PI signal for the most stable and biologically relevant keto-amino tautomers of guanine seems to support this heuristic conjecture. It is intriguing that the keto-amino tautomers of guanine are distinguished from the other tautomers by two competing mechanisms of ultrafast excited-state deactivation.

Acknowledgment. The authors thank Professor Andrzej L. Sobolewski for many stimulating discussions. This work has been supported by the Deutsche Forschungsgemeinschaft (DFG) through SFB 749. S.Y. acknowledges support by a fellowship of the Alexander von Humboldt Foundation. We thank the Leibniz-Rechenzentrum der Bayerischen Akademie der Wissenschaften (LRZ) for substantial allocation of computing time.

Supporting Information Available: Cartesian coordinates of optimized geometries of energy minima and conical intersections. Molecular orbitals at the conical intersection geometries. This material is available free of charge via the Internet at http://pubs.acs.org.

References and Notes

(1) Cadet, J.; Vigny, P. In *Bioorganic Photochemistry*; Morrison, H., Ed.; Wiley: New York, 1990; Vol. 1, p 1.
(2) Crespo-Hernández, C. E.; Cohen, B.; Hare, P. M.; Kohler, B. *Chem. Rev.* **2004**, *104*, 1977.
(3) Kang, H.; Lee, K. T.; Jung, B.; Ko, Y. J.; Kim, S. K. *J. Am. Chem. Soc.* **2002**, *124*, 12958.
(4) Canuel, C.; Mons, M.; Piuzzi, F.; Tardivel, B.; Dimicoli, I.; Elhanine, M. *J. Chem. Phys.* **2005**, *122*, 074316.
(5) Nir, E.; Grace, L.; Brauer, B.; de Vries, M. S. *J. Am. Chem. Soc.* **1999**, *121*, 4896.
(6) Nir, E.; Kleinermanns, K.; Grace, L.; de Vries, M. S. *J. Phys. Chem. A* **2001**, *105*, 5106.
(7) Nir, E.; Janzen, C.; Imhof, P.; Kleinermanns, K.; de Vries, M. S. *J. Chem. Phys.* **2001**, *115*, 4604.
(8) Piuzzi, F.; Mons, M.; Dimicoli, I.; Tardivel, B.; Zhao, Q. *Chem. Phys.* **2001**, *270*, 205.
(9) Mons, M.; Dimicoli, I.; Piuzzi, F.; Tardivel, B.; Elhanine, M. *J. Phys. Chem. A* **2002**, *106*, 5088.
(10) Chin, W.; Mons, M.; Dimicoli, I.; Piuzzi, F.; Tardivel, B.; Elhanine, M. *Eur. Phys. J. D* **2002**, *20*, 347.
(11) Chin, W.; Mons, M.; Piuzzi, F.; Tardivel, B.; Dimicoli, I.; Gorb, L.; Leszczynski, J. *J. Phys. Chem. A* **2004**, *108*, 8237.
(12) Hanus, M.; Ryjáček, F.; Kabeláč, M.; Kubař, T.; Bogdan, T. V.; Trygubenko, S. A.; Hobza, P. *J. Am. Chem. Soc.* **2003**, *125*, 7678.
(13) Gorb, L.; Kaczmarek, A.; Gorb, A.; Sadlej, A. J.; Leszczynski, J. *J. Phys. Chem. B* **2005**, *109*, 13770.
(14) Shukla, M. K.; Leszczynski, J. *Chem. Phys. Lett.* **2006**, *429*, 261.
(15) Liang, W.; Li, H.; Hu, X.; Han, S. *Chem. Phys.* **2006**, *328*, 93.
(16) Choi, M. Y.; Miller, R. E. *J. Am. Chem. Soc.* **2006**, *128*, 7320.
(17) Mons, M.; Piuzzi, F.; Dimicoli, I.; Gorb, L.; Leszczynski, J. *J. Phys. Chem. A* **2006**, *110*, 10921.
(18) Seefeld, K.; Brause, R.; Häber, T.; Kleinermanns, K. *J. Phys. Chem. A* **2007**, *111*, 6217.
(19) Saigusa, H. *J. Photochem. Photobiol. C* **2006**, *7*, 197.
(20) Ismail, N.; Blancafort, L.; Olivucci, M.; Kohler, B.; Robb, M. A. *J. Am. Chem. Soc.* **2002**, *124*, 6818.
(21) Sobolewski, A. L.; Domcke, W.; Dedonder-Lardeux, C.; Jouvet, C. *Phys. Chem. Chem. Phys.* **2002**, *4*, 1093.
(22) Sobolewski, A. L.; Domcke, W. *Eur. Phys. J. D* **2002**, *20*, 369.

(23) Merchán, M.; Serrano-Andrés, L. *J. Am. Chem. Soc.* **2003**, *125*, 8108.
(24) Langer, H.; Doltsinis, N. L. *Phys. Chem. Chem. Phys.* **2003**, *5*, 4516.
(25) Langer, H.; Doltsinis, N. L. *Phys. Chem. Chem. Phys.* **2004**, *6*, 2742.
(26) Matsika, S. *J. Phys. Chem. A* **2004**, *108*, 7584.
(27) Blancafort, L.; Robb, M. A. *J. Phys. Chem. A* **2004**, *108*, 10609.
(28) Marian, C. M. *J. Chem. Phys.* **2005**, *122*, 104314.
(29) Perun, S.; Sobolewski, A. L.; Domcke, W. *J. Am. Chem. Soc.* **2005**, *127*, 6257.
(30) Perun, S.; Sobolewski, A. L.; Domcke, W. *Chem. Phys.* **2005**, *313*, 107.
(31) Nielsen, S. B.; Sølling, T. I. *ChemPhysChem* **2005**, *6*, 1276.
(32) Matsika, S. *J. Phys. Chem. A* **2005**, *109*, 7538.
(33) Chen, H.; Li, S. *J. Phys. Chem. A* **2005**, *109*, 8443.
(34) Ritze, H.-H.; Lippert, H.; Samoylova, E.; Smith, V. R.; Hertel, I. V.; Radloff, W.; Schultz, T. *J. Chem. Phys.* **2005**, *122*, 224320.
(35) Langer, H.; Doltsinis, N. L.; Marx, D. *ChemPhysChem* **2005**, *6*, 1734.
(36) Blancafort, L.; Cohen, B.; Hare, P. M.; Kohler, B.; Robb, M. A. *J. Phys. Chem. A* **2005**, *109*, 4431.
(37) Tomić, K.; Tatchen, J.; Marian, C. M. *J. Phys. Chem. A* **2005**, *109*, 8410.
(38) Zgierski, M. Z.; Patchkovskii, S.; Fujiwara, T.; Lim, E. C. *J. Phys. Chem. A* **2005**, *109*, 9384.
(39) Zgierski, M. Z.; Patchkovskii, S.; Lim, E. C. *J. Chem. Phys.* **2005**, *123*, 081101.
(40) Blancafort, L. *J. Am. Chem. Soc.* **2006**, *128*, 210.
(41) Serrano-Andrés, L.; Merchán, M.; Borin, A. C. *Chem. Eur. J.* **2006**, *12*, 6559.
(42) Perun, S.; Sobolewski, A. L.; Domcke, W. *Mol. Phys.* **2006**, *104*, 1113.
(43) Serrano-Andrés, L.; Merchán, M.; Borin, A. C. *Proc. Natl. Acad. Sci. U.S.A.* **2006**, *103*, 8691.
(44) Chen, H.; Li, S. *J. Chem. Phys.* **2006**, *124*, 154315.
(45) Chen, H.; Li, S. *J. Phys. Chem. A* **2006**, *110*, 12360.
(46) Perun, S.; Sobolewski, A. L.; Domcke, W. *J. Phys. Chem. A* **2006**, *110*, 13238.
(47) Merchán, M.; González-Luque, R.; Teresa, C.; Serrano-Andrés, L.; Rodríguez, E.; Reguero, M.; Peláez, D. *J. Phys. Chem. B* **2006**, *110*, 26471.
(48) Gustavsson, T.; Bányász, Á.; Lazzarotto, E.; Markovitsi, D.; Scalmani, G.; Frisch, M. J.; Barone, V.; Improta, R. *J. Am. Chem. Soc.* **2006**, *128*, 607.
(49) Gustavsson, T.; Sarkar, N.; Lazzarotto, E.; Markovitsi, D.; Barone, V.; Improta, R. *J. Phys. Chem. B* **2006**, *110*, 12843.
(50) Zgierski, M. Z.; Patchkovskii, S.; Lim, E. C. *Can. J. Chem.* **2007**, *85*, 124.
(51) Yamazaki, S.; Kato, S. *J. Am. Chem. Soc.* **2007**, *129*, 2901.
(52) Zgierski, M. Z.; Patchkovskii, S.; Fujiwara, T.; Lim, E. C. *Chem. Phys. Lett.* **2007**, *440*, 145.
(53) Marian, C. M. *J. Phys. Chem. A* **2007**, *111*, 1545.
(54) Zgierski, M. Z.; Fujiwara, T.; Kofron, W. G.; Lim, E. C. *Phys. Chem. Chem. Phys.* **2007**, *9*, 3206.
(55) Kistler, K. A.; Matsika, S. *J. Phys. Chem. A* **2007**, *111*, 2650.
(56) Blancafort, L.; Migani, A. *J. Photochem. Photobiol. A* **2007**, *190*, 283.
(57) Hudock, H. R.; Levine, B. G.; Thompson, A. L.; Satzger, H.; Townsend, D.; Gador, N.; Ullrich, S.; Stolow, A.; Martínez, T. J. *J. Phys. Chem. A* **2007**, *111*, 8500.
(58) Kistler, K. A.; Matsika, S. *J. Phys. Chem. A* **2007**, *111*, 8708.
(59) Serrano-Andrés, L.; Merchán, M.; Borin, A. C. *J. Am. Chem. Soc.* **2008**, *130*, 2473.
(60) Klessinger, M.; Michl, J. *Excited States and Photochemistry of Organic Molecules*; VCH: New York, 1995.
(61) Bernardi, F.; Olivucci, M.; Robb, M. A. *Chem. Soc. Rev.* **1996**, *25*, 321.
(62) Yarkony, D. R. *Acc. Chem. Res.* **1998**, *31*, 511.
(63) Yarkony, D. R. *J. Phys. Chem. A* **2001**, *105*, 6277.
(64) Domcke, W., Yarkony, D. R., Köppel, H. , Eds. *Conical Intersections: Electronic Structure, Dynamics and Spectroscopy*; World Scientific: Singapore, 2004.
(65) Werner, H.-J. et al. *MOLPRO*, version 2006.1, a package of ab initio programs; 2006; see http://www.molpro.net.
(66) Dunning, T. H., Jr. ; Hay, P. J. In *Methods of Electronic Structure Theory*; Schaefer, H. F., III, Ed.; Plenum: New York, 1977.
(67) Celani, P.; Werner, H.-J. *J. Chem. Phys.* **2000**, *112*, 5546.
(68) Roos, B. O.; Andersson, K. *Chem. Phys. Lett.* **1995**, *245*, 215.
(69) Dunning, T. H., Jr *J. Chem. Phys.* **1971**, *55*, 716.
(70) Sobolewski, A. L.; Domcke, W. *Phys. Chem. Chem. Phys.* **2004**, *6*, 2763.
(71) Sobolewski, A. L.; Domcke, W. *Chem. Phys. Lett.* **1999**, *315*, 293.
(72) Sobolewski, A. L.; Domcke, W. *Chem. Phys.* **2000**, *259*, 181.
(73) Sobolewski, A. L.; Domcke, W. *J. Phys. Chem. A* **2001**, *105*, 9275.
(74) Sagan, C. *J. Theor. Biol.* **1973**, *39*, 195.
(75) Abo-Riziq, A.; Grace, L.; Nir, E.; Kabelac, M.; Hobza, P.; de Vries, M. S. *Proc. Natl. Acad. Sci. U.S.A.* **2005**, *102*, 20.
(76) Sobolewski, A. L.; Domcke, W. *Europhysicsnews* **2006**, *37*, 20.

JP802759V